Molecular Biology of the Cell
Vol. 18, 2356–2366, June 2007

Increased Apoptosis and Skewed Differentiation in Mouse Embryonic Stem Cells Lacking the Histone Methyltransferase Mll2[D]

Sandra Lubitz,* Stefan Glaser,*† Julia Schaft,*‡ A. Francis Stewart,* and Konstantinos Anastassiadis*§

*Genomics Group, BioInnovations Zentrum, and §Centre for Regenerative Therapies Dresden, Technische Universität Dresden, 01307 Dresden, Germany

Submitted December 1, 2006; Revised March 14, 2007; Accepted March 30, 2007
Monitoring Editor: Wendy Bickmore

Epigenetic regulation by histone methyltransferases provides transcriptional memory and inheritable propagation of gene expression patterns. Potentially, the transition from a pluripotent state to lineage commitment also includes epigenetic instructions. The histone 3 lysine 4 methyltransferase Mll2/Wbp7 is essential for embryonic development. Here, we used embryonic stem (ES) cell lines deficient for Mll2 to examine its function more accurately. *Mll2*−/− ES cells are viable and retain pluripotency, but they display cell proliferation defects due to an enhanced rate of apoptosis. Apoptosis was not relieved by caspase inhibition and correlated with decreased *Bcl2* expression. Concordantly, Mll2 binds to the *Bcl2* gene and H3K4me³ levels are reduced at the binding site when Mll2 is absent. In vitro differentiation showed delays along representative pathways for all three germ layers. Although ectodermal delays were severe and mesodermal delays persisted at about three days, endodermal differentiation seemed to recover and overshoot, concomitant with prolonged *Oct4* gene expression. Hence, Mll2 is not required for ES cell self-renewal or the complex changes in gene expression involved in lineage commitment, but it contributes to the coordination and timing of early differentiation decisions.

INTRODUCTION

Distinct cell types are characterized by specific gene expression profiles, which are established during development and thereafter maintained. Although gene expression is controlled by transcription factors, it is also dependent upon the underlying chromatin structure, which is inherited during S phase by the reproduction of local histone modifications (Margueron *et al*., 2005; Boyer *et al*., 2006a; Meshorer and Misteli, 2006). Of various histone modifications, methylation of lysines seems to be central to this process of inheritance and epigenetic regulation.

The Polycomb (PcG) and trithorax (trxG) groups are part of a widely conserved cell memory system that stabilizes cell identity by restricting and maintaining transcription patterns set in early embryonic life, throughout development and in adulthood (Ringrose and Paro, 2004; Lin and Dent, 2006). Whereas the PcG is involved in gene repression and silencing, the trxG counteracts PcG function and maintains specific gene activity. Both groups include multiprotein complexes that methylate lysines in histone 3. Specifically, PcG action involves methylation at lysine 27 (H3K27) (Cao *et al*., 2002; Czermin *et al*., 2002; Kuzmichev *et al*., 2002; Muller *et al*., 2002), and trxG action involves methylation at lysine 4 (H3K4) (Roguev *et al*., 2001; Milne *et al*., 2002), thereby directing the inheritance of gene silencing or gene activity, respectively. Consequently the genetic opposition of PcG and trxG could be, at least in part, due to a biochemical competition for the methylated status of the H3 tail. Recent evidence from embryonic stem (ES) cells shows that a key set of genes involved in lineage commitment is dually H3K4 and H3K27 methylated (Azuara *et al*., 2006; Bernstein *et al*., 2006; Boyer *et al*., 2006b; Lee *et al*., 2006). This concords with the intimate functional opposition between PcG and trxG (Klymenko and Muller, 2004).

Both PcG and trxG proteins are well conserved in metazoans. The founding member of the trxG is trithorax (TRX), which maintains homeotic gene expression in *Drosophila* throughout embryonic development (Breen and Harte, 1993). Mammals have two orthologues of TRX, called mixed lineage leukemia (Mll) and Mll2, which is also called Wbp7. These proteins are very large, and they carry a variety of conserved sequence motifs, the most prominent being a SET domain, which methylates H3K4.

Several histone methyltransferases, such as *G9a* (Tachibana *et al*., 2002), *Eset* (Dodge *et al*., 2004) *Mll* (Yagi *et al*., 1998; Yu *et al*., 1998), and *Mll2* (Glaser *et al*., 2006), have been mutated in the mouse to reveal that each is important in early devel-

This article was published online ahead of print in *MBC in Press* (http://www.molbiolcell.org/cgi/doi/10.1091/mbc.E06–11–1060) on April 11, 2007.

[D] The online version of this article contains supplemental material at *MBC Online* (http://www.molbiolcell.org).

Present addresses: † The Walter and Eliza Hall Institute for Medical Research, Cancer and Haematology Division, 1G Royal Parade, Parkville, Melbourne, VIC 3050, Australia; ‡ Sydney IVF, 4 O'Connell St., Sydney 2000, Australia.

Address correspondence to: A. Francis Stewart (francis.stewart@biotec.tu-dresden.de).

Abbreviations used: APC, allophycocyanin; EB, embryoid body; ES, embryonic stem; F/F, FLP-rescued; H3K4, histone 3 lysine 4; H3K27, histone 3 lysine 27; LIF, leukemia inhibitory factor; Mll, mixed lineage leukemia; PcG, Polycomb group; trxG, trithorax group.

opment, albeit in different ways. Homozygous *mll2* mutant embryos fail to develop beyond about E9.5 because of severe, widespread defects, which seem to be distinct from the defects observed in homozygous *mll* mutant embryos (Glaser *et al*., 2006). This suggests that these two factors regulate different genes. However, no evidence for cell type specificity in the phenotypes was observed until well after gastrulation. This further suggests that these factors are redundant for lineage commitment in early development but that they are required at a later stage, potentially to maintain and propagate specific decisions.

Here, we examine the roles of Mll2 in lineage commitment and differentiation more accurately. The properties and abilities of *mll2*−/− ES cells were examined for the undifferentiated state as well as for differentiation along paths representative for each of the three germ layers. Although Mll2 is dispensable for ES cell self-renewal, it is needed for the correct regulation of apoptosis and the timing of developmental processes.

MATERIALS AND METHODS

Generation of mll2 Mutant and Control ES Cell Lines

To make *mll2*−/− cells, heterozygously targeted E14.1 *mll2*+/− cells (Glaser *et al*., 2006) were electroporated with the same targeting vector except the neomycin resistance gene was replaced by hygromycin by using Red/ET recombination (Zhang *et al*., 1998; Testa *et al*., 2004). Double-targeted ES cell clones were selected for G418 (250 μg/ml, Geneticin; Invitrogen, Karlsruhe, Germany) and hygromycin (200 μg/ml; Roche Diagnostics, Mannheim, Germany). Correct targeting of homozygous *mll2*−/− clones was determined by Southern blot by using EcoRI and a 600-base pair EcoRI/BglI probe fragment (BE580). To rescue Mll2 expression, *mll2*−/− ES cells were transiently transfected with a pCAGGS-FLPe expression plasmid by electroporation (Schaft *et al*., 2001) and selected with 1 μg/ml puromycin (Sigma-Aldrich, Taufkirchen, Germany) for 48 h. FLP-rescued clones were checked by Southern blot (BE580 probe) and polymerase chain reaction (PCR) analysis for loss of the targeting cassettes. FLP-rescue was additionally evaluated by loss of resistance to hygromycin and G418 selection. Rescued clones were checked for unwanted genomic integration of the FLPe expression vector, and those clones, totaling approximately one third of the dually FLP recombined clones, were excluded. E14.1 Mll2-TAP ES cells were generated by inserting a TAP cassette into the first exon of the endogenous *mll2* locus (Testa *et al*., 2003).

ES Cell Culture Conditions and In Vitro Differentiation

ES cell clones were maintained on mitomycin-treated mouse embryonic fibroblasts (MEFs) in standard ES cell medium (DMEM, 15% fetal calf serum [FCS], 2 mM L-glutamine, 1 mM sodium pyruvate, 1% penicillin/streptomycin, and 100 μM nonessential amino acids (all from Invitrogen), 100 μM β-mercaptoethanol (Sigma-Aldrich) containing leukemia inhibitory factor (LIF).

Cardiac differentiation was evoked by culturing ES cell clones as embryoid bodies (EBs) according to the hanging drop method (Maltsev *et al*., 1993). Drops of cardiac differentiation medium (DMEM, 20% FCS, 2 mM L-glutamine, 100 μM nonessential amino acids, 1% penicillin/streptomycin, and 100 μM β-mercaptoethanol) containing 1×10^3 or 2×10^3 ES cells were placed onto the lids of culture dishes. After 48 h, EBs were transferred onto bacterial plates and cultured in suspension for another 2 d. On day 5, EBs were plated separately onto gelatin-coated 24-well plates and checked daily for spontaneous contractile activity (up to day 25). Single cardiac myocytes were prepared from EB outgrowths on day 21. Contractile areas of EBs were dissected, dissociated (Maltsev *et al*., 1993), and processed for cardiac-specific immunoreactivity by using mouse monoclonal antibodies against desmin (D3) and titin (9D10) (Developmental Studies Hybridoma Bank, Iowa City, IA).

In vitro differentiation into neurons was achieved according to published methods with some modifications (Li *et al*., 1998; Ying *et al*., 2003). EBs were generated by mass culture in ES cell medium without LIF on nonadhesive bacterial grade dishes. Mass culture was started with $\sim 3 \times 10^6$ ES cells/10-cm plate, and cells were cultured in suspension until 96 h (day 4). After addition of 10^{-6} M all-trans retinoic acid (Sigma-Aldrich) incubation was continued for 96 h (day 8). Cell aggregates were then allowed to attach onto adhesive gelatin-coated tissue culture dishes. On day 10, the adherent EBs were dissociated with 4× concentrated trypsin. Single cells were plated out at 1×10^5 cells (for wild-type [wt] and FLP-rescued) or 2×10^5 cells per 24-well (for *mll2*−/−) onto poly-D-lysine/laminin-coated (Sigma-Aldrich) glass coverslips. The next day, the medium was changed to N2B27 (1:1 mixture of DMEM/F-12 and neurobasal medium, 1× N2, 1× B27, 2 mM L-glutamine (all from Invitrogen). Dissociated cells were maintained in N2B27 medium (up to day 36) before being processed for immunocytochemistry.

The method for in vitro differentiation to endoderm was adapted from Lumelsky *et al*. (2001). A mass culture of EBs was started with 1.5×10^6 ES cells in DMEM, 20% FCS, 1% penicillin/streptomycin, and 100 μM β-mercaptoethanol. After 96 h, EBs were plated onto gelatinized tissue culture plates in the same media. The next day, the medium was changed to serum-free ITSF medium (Lumelsky *et al*., 2001) and incubation was continued for 6 d, with daily media exchange. On day 12 the medium was changed to serum-free N2 medium (DMEM/F-12, 1× N2, 1× B27, 10 ng/ml basic fibroblast growth factor (all from Invitrogen), 1 μg/ml laminin (Sigma-Aldrich) for expansion of endodermal cell types.

Cell Proliferation and Cell Cycle Analysis

To assay proliferation, ES cells were seeded onto mitomycin-treated MEFs at 2.3×10^4 cells (in triplicates) in six-well dishes and counted on five consecutive days. Proliferation of cells upon the first days of differentiation was determined with EBs. Mass culture of EBs was started with 3×10^5 ES cells per bacterial dish by using standard ES medium without LIF. Resulting EBs were trypsinized and counted on four consecutive days (in triplicates). For apoptosis studies, ES cells were grown in the presence of 40 μM Z-VAD-FMK general caspase inhibitor (BIOMOL Research Laboratories, Hamburg, Germany) prepared in dimethyl sulfoxide (DMSO) or the same vol/vol pure DMSO and counted on four consecutive days (in triplicates).

For bromodeoxyuridine (BrdU) incorporation studies, ES cell clones were spread without feeder cells and grown with 10 μM BrdU ES cell medium for various times (0.5–22 h). BrdU incorporation was detected by flow cytometry using a monoclonal mouse antibody to BrdU (Developmental Studies Hybridoma Bank). Fluorescence-activated cell sorting (FACS) analysis was performed using a FACS Aria station (BD Biosciences, Heidelberg, Germany) with DiVa software.

For cell cycle analysis, asynchronously growing ES cells were fixed with ethanol and stained with 1 μg/ml propidium iodide (PI) containing 0.1 mg/ml RNase A (both from Sigma-Aldrich). Cells were analyzed by flow cytometry to determine G1, S, and G2/M cell cycle distribution with ModFit software (Verity Software House, Topsham, ME). Cell cycle length was assigned by time-lapse analysis. Time-lapse movies of exponentially growing ES cells were documented on an upright Axiovert 200M microscope with a digital camera. ES cells were cultured in a heated culture chamber at 37°C/5% CO_2 during imaging and recorded for 24 h. Images were taken with a sampling interval of 5 min. MetaMorph software version 5.0 was used to align the stacks in time-lapse movies.

Apoptosis Assays

Terminal deoxynucleotidyltransferase-mediated dUTP-biotin nick end labeling (TUNEL) staining was performed with the In Situ Cell Death Detection kit (Roche Diagnostics). ES cells and differentiating cells were fixed and incubated with TUNEL reaction mixture according to the manufacturer's instructions.

Annexin V staining was used to define the basal levels of apoptosis for each ES cell clone. ES cells were grown on mitomycin-treated feeder cells for 22 h before they were harvested and stained with allophycocyanin-labeled Annexin V (Annexin V-APC) for flow cytometric analysis. As a positive control, wild-type ES cells were induced with 12 μM camptothecin (Sigma-Aldrich) for 6 h to undergo apoptosis. Cells were trypsinized and single cell suspensions (1×10^5 cells/clone) were stained with 0.5 μg/ml PI and Annexin V-APC (dilution 1:20) according to the manufacturer's instructions. As a control, Annexin V binding was blocked with 5 μg of unlabeled recombinant Annexin V protein per 1×10^5 ES cells before Annexin V-APC staining. Cells were subjected to flow cytometry and analyzed by DiVa software. For FACS sorting of viable and apoptotic cell populations, live *mll2*−/− ES cells were stained with Annexin V-APC and PI and separated on a FACS Aria station. In total, 3×10^5 Annexin V-positive and 5×10^5 Annexin V-negative *mll2* mutant ES cells was used to extract total RNA for reverse transcription analysis.

Expression Analysis by Western Blotting

For preparation of crude protein extracts, ES cell clones were grown without feeder cells on gelatin-coated plates. Protein extracts were prepared from $\sim 1 \times 10^7$ ES cells. Cell pellets were resuspended in protein extraction buffer (20 mM HEPES, pH 8.0, 350 mM NaCl, 2 mM EDTA, 10% glycerol, 0.1% Tween 20, and 1% protease inhibitor cocktail; Sigma-Aldrich) and subjected to three successive freeze and thaw cycles. Crude protein extracts were resolved on 5% (for detection of Mll2) or 10% (for detection of β-actin) polyacrylamide gels and transferred to PROTRAN (Dassel, Germany) nitrocellulose membranes by semidry blotting. Membranes were incubated with a rabbit immunoglobulin G (IgG) polyclonal antibody raised against Mll2 (Glaser *et al*., 2006) and with an β-actin antibody (Sigma-Aldrich), which served as a loading control. Signals were detected using the SuperSignal West Femto kit (Pierce Chemical, Rockford, IL). Antibodies used for HMTase activity studies are specific for histone $H3K4me^3$ and $H3K9me^2$ (both from Abcam, Cambridge, United Kingdom). Ponceau staining of protein gels served as a loading control.

Immunocytochemistry

Cells were fixed with 4% formaldehyde, permeabilized with 0.5% Triton X-100, and blocked with 3% bovine serum albumin before antibody staining. Primary antibodies were as follows: anti-desmin (D3), anti-titin (9D10), anti-BrdU (G3G4), anti-stage–specific embryonic antigen 1 (SSEA1) (MC-480), anti-nestin (Rat-401), anti-neurofilament 165-kDa (2H3) (all from Developmental Studies Hybridoma Bank), anti-β-tubulin class III (TuJI) (BAbCO, Richmond, CA), and anti-microtubule-associated protein 2 (MAP2) (Sigma-Aldrich). After incubation with specific secondary antibodies, cell nuclei were counterstained with 0.1 μg/ml 4,6-diamidino-2-phenylindole (DAPI), and cells were mounted with Prolong Antifade kit (MoBiTec, Göttingen, Germany).

Reverse Transcription and Quantitative PCR (qPCR) Analysis

For detection of developmental and lineage-specific mRNAs expressed during in vitro ES cell differentiation, total RNA was isolated using TRI-reagent (Sigma-Aldrich) or the RNeasy Kit (QIAGEN, Hilden, Germany). DNase I-treated total RNA (1 μg) was reverse transcribed using the SuperScript III First Strand Synthesis system (Invitrogen). For quantitative PCR analysis, cDNA was diluted 1:5–1:20 as a template. qPCR reactions were run on a Stratagene MX4000 multiplex PCR instrument according to the manufacturer's instructions. qPCR analyses were done in triplicates, and Ct values were normalized against the internal control genes *tubulin* or *ribosomal protein L19* (*RPL19*). Primer sequences and the length of amplified products are given in Supplemental Material. -Fold differences in expression levels were calculated according to the $2^{-\Delta\Delta Ct}$ method (Livak and Schmittgen, 2001).

Chromatin Immunoprecipitation

ES cells were grown without feeder layers for 48 h and fixed with 1% formaldehyde for 10 min at room temperature. Pellets of 2–3 $\times$ 10^6 cells were lysed with SDS lysis buffer (1% SDS, 10 mM EDTA, and 50 mM Tris-HCl, pH 8.1) in the presence of 1$\times$ protease inhibitors (Complete; Roche Diagnostics). Cell lystates were sonicated to an average genomic fragment length of 300–800 base pairs. Because of the lack of a functional Mll2 antibody, E14.1 Mll2-TAP ES cell lysates were precipitated with IgG-Sepharose beads (GE Healthcare, Freiburg, Germany) overnight at +4°C. IgG beads recognize the protein A part of the TAP-tag, thereby precipitating Mll2 target genes. For $H3K4me^3$, cell lysates were incubated with 5 μl of $H3K4me^3$ antibody (Abcam) overnight and precipitated with GammaBinding G-Sepharose beads (GE Healthcare) for 1 h at + 4°C. Beads were washed with low salt immune complex buffer (0.1% SDS, 1% Triton X-100, 2 mM EDTA, 20 mM Tris-HCl, pH 8.1, and 150 mM NaCl), high salt immune complex buffer (0.1% SDS, 1% Triton X-100, 2 mM EDTA, 20 mM Tris-HCl, pH 8.1, and 500 mM NaCl), LiCl immune complex buffer (0.25 M LiCl, 1% NP-40, 1% deoxycholic acid, 1 mM EDTA, and 100 mM Tris-HCl, pH 8.1) and TE buffer. Elution of immunoprecipitates from the beads was performed with 1% SDS, 0.1 M $NaHCO_3$. Eluates were incubated for 6 h at 65°C to reverse cross-links followed by phenol/chloroform DNA extraction. Immunoprecipitated DNA and input DNA were analyzed by quantitative PCR.

RESULTS

Generation, Rescue, and Characterization of mll2−/− ES Cells

Mll2 knockout ES cells were generated by inserting a multipurpose cassette into the first intron of the endogenous *mll2* locus (Glaser *et al*., 2006). Targeting of the second allele with the same construct after exchanging the selectable marker (hygromycin for neomycin) created a null mutation of *mll2*. The targeting frequency for the second allele was 3% (the first allele had been 8.4% (Glaser *et al*., 2006). The *mll2* targeting cassette is flanked by FRT sites and contains a synthetic exon and a polyadenylation signal, which captures and terminates *mll2* expression (Figure 1, A and B). To exclude the possibility that phenotypic changes observed with *mll2−/−* ES cells were due to secondary mutagenesis during gene targeting, rather than the loss of Mll2 function, the cells were rescued by FLPe-recombination, which deleted the targeting cassette thereby restoring *mll2* expression (Figure 1, C and D). Two independent *mll2−/−* ES cell clones were used for experimental analysis and rescued by FLPe-mediated recombination. Both clones revealed similar results with an FLPe-recombination rate of ~10%, including 7.5% heterozygously and 2.5% homozygously FLPe-recombined clones. Both wild-type and homozygously FLP-rescued ES cells, referred to hereafter as "FLP-rescued" or F/F, served as a control for the *mll2−/−* phenotype.

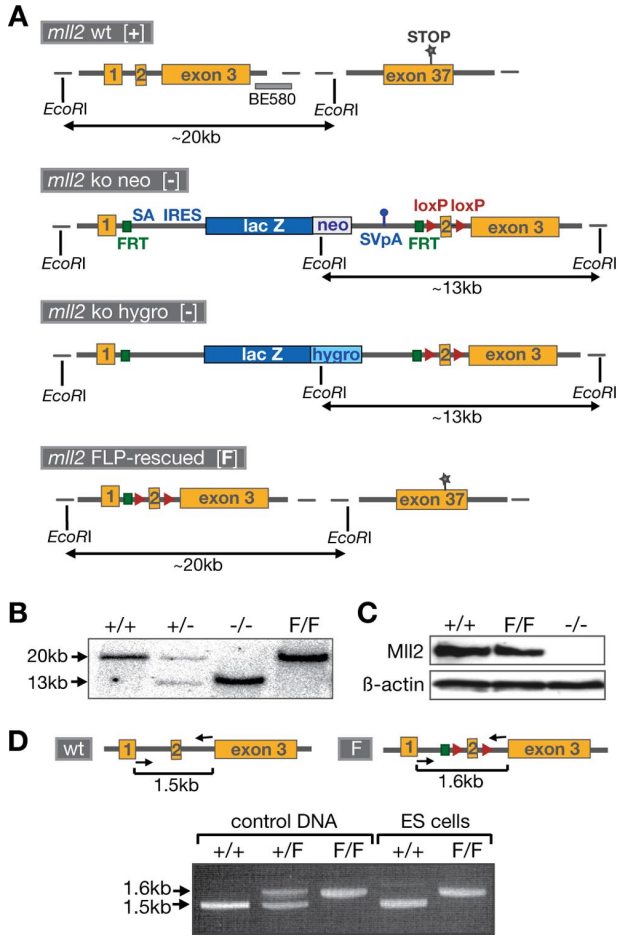

Figure 1. Targeted disruption of the *mll2* gene in ES cells. (A) Schematic diagram of the endogenous *mll2* locus. Homozygous *mll2* mutant ES cells were generated by insertion of a lacZ-neo and a lacZ-hygro targeting cassette into the first intron of *mll2*. The targeting cassette contains a splice acceptor (SA), an internal ribosomal entry site (IRES), a selection cassette (lacZ-neo or lacZ-hygro), and a polyadenylation signal (SVpA). Green rectangles indicate FRT sites (target sites for FLPe recombinase); red triangles indicate loxP sites (target sites for Cre recombinase). FLPe mediated recombination between the two FRT sites leads to removal of the targeting cassette in *mll2* mutant cells and restores the wild-type situation, except for one FRT site and two loxP sites remaining in intronic positions. Rescued alleles are indicated as F for FLP-recombined. (B) Southern blot analysis of DNA from ES cell clones. Genomic DNA was digested with EcoRI and hybridized with a 600-base pair EcoRI/BglI probe (BE580), which anneals downstream of the simian virus 40 polyA signal. The probe detects a 20-kb fragment in wild-type (+/+) and a 13-kb fragment in *mll2* mutant (−/−) ES cells. ES cells heterozygous for the mutation (+/−) show both the 20- and 13-kb band. Homozygously FLP-rescued ES cells (F/F) reveal a single ~20-kb band. (C) Western blot analysis of ES cell protein extracts was performed using purified antiserum raised against Mll2. An antibody to β-actin served as a loading control. (D) PCR analysis of FLP-rescued ES cells. DNA from mouse wild-type (+/+) ES cells, or heterozygously (+/F) and homozygously (F/F) FLP-recombined somatic cells (mouse tail DNA) was used as a control. Using specific primer pairs spanning the region between exon 1 and exon 3 of *mll2*, FLP-rescued alleles revealed a 1.6-kb band, which was distinguishable from the 1.5-kb wild-type band upon gel electrophoresis.

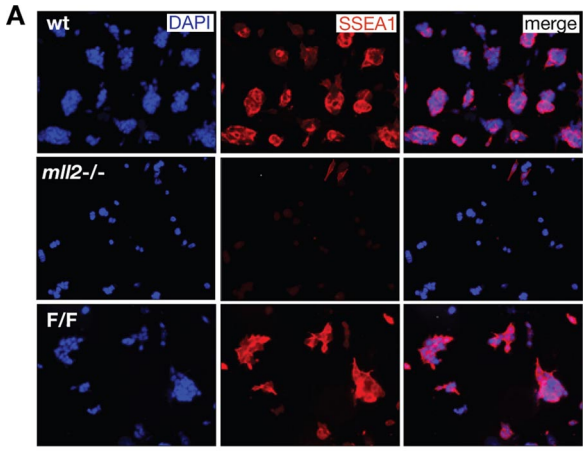

	Oct4	SSEA1
wt	95%	85%
F/F	93%	69%
-/-	89%	4%

Figure 2. Loss of the SSEA1 epitope in Mll2-deficient ES cells. (A) Colonies of undifferentiated wt, F/F, and *mll2* mutant (−/−) ES cells were processed for SSEA1-specific immunoreactivity. Nuclei were counterstained with DAPI. Magnification, 20×. (B) SSEA1 epitope expression in ES cell clones. Undifferentiated wt, F/F, and −/− ES cells were stained with anti-SSEA1 and anti-Oct4 and analyzed by flow cytometry. Percentages of SSEA1- and Oct4-positive cells per clone result from analysis of 5000 events. (C) Quantitative PCR analysis of *Fut9* gene expression in Mll2-deficient cells. Undifferentiated (undiff.) and differentiating (day 4) wt, F/F, and *mll2*−/− ES cells were used. Ct values derived for each clone were normalized against the endogenous standard gene *tubulin*. Data are means of triplicate analysis; error bars represent SD.

To investigate Mll2 function in self-renewal, we first looked for expression of characteristic ES cell markers. SSEA1, also called Lewis X antigen [LeX]) is a marker for undifferentiated mouse embryonic stem cells, embryonic carcinoma cells, and primordial germ cells (Solter and Knowles, 1978; Muramatsu, 1988). An SSEA1-specific antibody revealed an unexpected decrease in SSEA1 labeling of *mll2*−/− ES cells. Wild-type and FLP-rescued ES cell colonies displayed SSEA1 antigen in immunofluorescence analysis, but only occasional *mll2*−/− ES cell colonies were SSEA1 positive (Figure 2A). This finding was confirmed for surface labeling by FACS analysis with an SSEA1-specific antibody. Whereas on average only 4% of *mll2*−/− ES cells were SSEA1 positive (Figure 2B), 85 or 69% SSEA1-positive cells were observed in wild-type or FLP-rescued ES cells, respectively. Because decreased SSEA1 expression could indicate loss of pluripotency, ES cell clones were double-labeled with an antibody against the pluripotency marker Oct4 (Nichols *et al*., 1998). All three ES cell clones displayed similar levels of Oct4 protein (Figure 2B). Maintenance of *Oct4* expression was confirmed by quantitative PCR analysis, which also showed no differences in *Nanog* expression levels (Supplemental Figure S1).

Apparently loss of the SSEA1 epitope could be due to a block in its synthesis pathway. Expression of the SSEA1 epitope in ES cells depends upon the enzymatic activity of α1,3-fucosyltransferase IX (Fut9) (Liu *et al*., 1999; Kudo *et al*., 2004). However, *Fut9* expression levels were not affected by the absence of Mll2 (Figure 2C). Furthermore, we found that *mll2*−/− blastocyst outgrowths showed variable SSEA1 expression, which was indistinguishable from heterozygote and wild-type blastocysts (data not shown). As noted previously (Solter and Knowles, 1978; Cui *et al*., 2004), we also cannot draw any conclusions about the functional relevance of SSEA1 expression.

Because Mll2 is a histone methyltransferase with specificity for H3K4, we looked at total H3K4 methylation levels in wild-type and *mll2*−/− cells by Western blotting. However, no differences in global H3K4 methylation in ES cells or differentiated cell types could be found (Supplemental Figure S2), indicating that other methyltransferases are responsible for bulk H3K4 methylation.

mll2−/− Cells Display a Proliferative Defect

Despite the loss of SSEA1, the morphology of *mll2*−/− colonies was virtually identical to wild-type and FLP-rescued ES cells unless mutant colonies were smaller. Therefore, proliferation rates were analyzed by counting cells over several days (Figure 3A). The growth of *mll2*−/− cultures was clearly retarded in the undifferentiated state and also during the first days of differentiation.

To determine the basis of the proliferation defect, we analyzed cell cycle parameters. Cells were incubated with BrdU for different times, stained with a BrdU antibody, and analyzed by flow cytometry. We observed no significant difference in BrdU incorporation between wild-type, FLP-rescued, and *mll2*−/− ES cells (Figure 3C). Likewise, immunostaining of undifferentiated ES cell colonies that were pulsed with BrdU showed no difference (Figure 3B). FACS analysis of wild-type, FLP-rescued, and *mll2*−/− ES cell clones upon propidium iodide staining revealed that cell cycle distribution was also unaffected by loss of Mll2. There was no significant difference in G1, S, G2, and M phase distribution between the three clones (Figure 3D). We also determined doubling times of each ES cell clone by videomicroscopy. Exponentially growing wild-type, FLP-rescued, and *mll2*−/− ES cells were monitored for 24 h, and dividing cells were tracked until they underwent the next mitotic division. Time-lapse movies revealed no difference in cell cycle length. All three clones showed an average cell cycle transition time of 13 h (Figure 3E).

Loss of Mll2 Leads to Increased Apoptosis

The first evidence for an enhanced rate of apoptosis in *mll2*−/− ES cells came from the time-lapse movies, which indicated that mutant ES cells are prone to cell death during or right after cell division. Mutant cells that underwent cell death showed characteristics of apoptosis, such as cell shrinkage, membrane blebbing, and apoptotic body formation (Figure 4A). TUNEL stainings of *mll2*−/− ES cells confirmed enhanced apoptosis rates (Figure 4B). Quantification of apoptosis was done by FACS analysis after staining for Annexin V. Annexin V analysis focuses on loss of the plasma membrane asymmetry as one of the earliest features of apoptosis. In early apoptotic cells, the membrane phospholipid phosphatidylserine is translocated to the outer leaflet of the plasma membrane, where it can be bound by Annexin V protein. According to this, exponentially growing *mll2*−/− ES cells were ~5% more apoptotic than wild-type ES cells (Figure 4C and Supplemental Figure S3A). Replicate analysis showed that this increase was statistically significant ($p < 0.025$). Importantly, levels of apoptosis reverted to normal values in FLP-rescued ES cells. Hence,

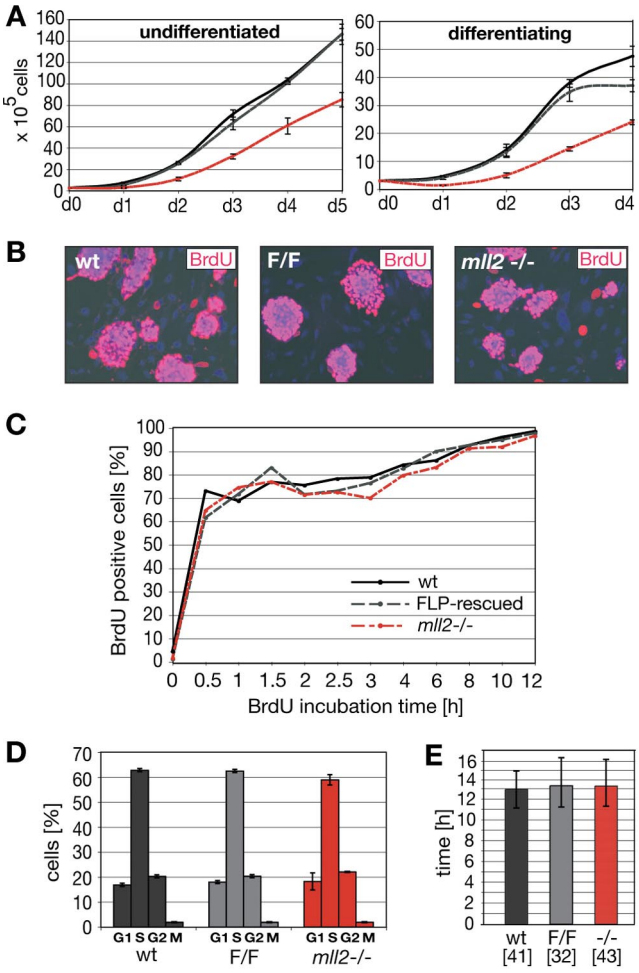

Figure 3. Proliferation and cell cycle analysis of *mll2* mutant ES cells. (A) Proliferation rates of undifferentiated and differentiating ES cell clones. Wild-type (black lines), FLP-rescued (dashed gray lines), and *mll2*−/− (dashed red lines) cells were counted for four or five consecutive days. Error bars represent SD of triplicate analyses. (B) Immunohistochemical detection of BrdU incorporation in ES cells. Cellular incorporation of BrdU during S phase was detected with an anti-BrdU antibody. (C) Flow cytometric analysis of BrdU incorporation in exponentially growing ES cells. Cells were labeled with BrdU for different times (up to 12 h). Incorporation of BrdU was measured over time by flow cytometry using a monoclonal anti-BrdU antibody. (D) Cell cycle distribution of ES cell clones. Exponentially growing ES cells were analyzed for cell cycle distribution by PI staining and flow cytometry. (E) Cell cycle length of undifferentiated ES cell clones. Time-lapse movies of growing ES cell clones were recorded for 24 h. Dividing ES cells were tracked for determination of cell cycle length. Numbers in brackets represent the number of monitored cell divisions per clone; error bars represent SD.

enhanced apoptosis in *mll2*−/− ES cells resulted from the loss of Mll2 function in these cells.

Increased Apoptosis Correlates with reduced Bcl2 Expression

Apoptotic pathways in ES cells have not yet been fully elucidated. Although these pathways differ from those observed in somatic cells, caspase dependence has been shown (Hakem *et al.*, 1998; Woo *et al.*, 1998; Yoshida *et al.*, 1998). To address whether the enhanced apoptosis was due to accelerated activation of caspases, undifferentiated ES cell clones were cultured in the presence of the broad-spectrum caspase inhibitor Z-VAD-FMK, which is a cell-permeable irreversible antagonist. The Z-VAD-FMK did not affect the morphology of wild-type, FLP-rescued, or *mll2*−/− ES cell clones. Although being effective (Supplemental Figure S3B), the inhibitor failed to restore the retarded growth rates of *mll2*−/− ES cultures (Supplemental Figure S3C).

The expression of several apoptotic marker genes was examined after FACS sorting of viable and apoptotic ES cell populations after Annexin V staining. Quantitative PCR analysis revealed an approximate threefold down-regulation of the antiapoptotic marker gene *Bcl2* in both viable (Annexin V-negative) and apoptotic (Annexin V-positive) *mll2*−/− cells (Figure 4D). Normally, Bcl-2 activity stabilizes the mitochondrial membrane potential and prevents the release of apoptogenic factors from the mitochondria to the cytosol (Kluck *et al.*, 1997; Daugas *et al.*, 2000). Moreover, expression of the proapoptotic marker genes, *Caspase-8* and *apoptosis inducing factor* (*AIF*), was slightly increased in apoptotic *mll2*−/− cells. Caspase-8 is an initiator caspase that proteolytically cleaves and activates other caspases. AIF is an apoptotic protease, which is held in mitochondria by Bcl-2 (Susin *et al.*, 1999). When AIF is translocated to the nucleus, it causes the chromatin condensation and DNA fragmentation that characterize apoptosis (Daugas *et al.*, 2000).

AIF-mediated apoptosis can be induced by increased expression of *Parp1* [*poly (ADP-ribose) polymerase-1*], because nuclear translocation of AIF requires Parp1 protein (Yu *et al.*, 2002). However, the number of *Parp1* transcripts was not altered in *mll2* mutant cells (Supplemental Figure S3D). In addition, transcription of genes for the apoptotic protease-activating factor (Apaf1) and caspase-9, which form a multiprotein caspase-activating apoptosomal complex together with cytochrome *c*, were unaffected, as was transcription of caspase-3 (Supplemental Figure S3D).

To confirm that *Bcl2* was down-regulated when Mll2 is absent, we looked at mRNA levels in an in vitro differentiation time course (Figure 4E) as well as in embryos taken at embryonic day E7.5 and E8.5 (Figure 4F). Both analyses showed that *Bcl2* expression was decreased in Mll2-deficient cells. Together, it is likely that increased apoptosis in *mll2* mutant cells is due to reduced *Bcl2* expression levels.

Mll2 Binds to the Bcl2 Gene

Because *Bcl2* expression was reduced in the absence of Mll2, we explored the possibility that Mll2 directly regulates this gene. Because of the absence of a suitable antibody, chromatin immunoprecipitation was done with an ES cell line that had the TAP-tag targeted to the N terminus of Mll2 (Testa *et al.*, 2003). On TAP-IP, a region near the 5′ end of *Bcl2* was specifically retrieved (Figure 4G). Consequently, we looked at H3K4me^3 in the same region and observed a substantial decrease (Figure 4H). These data demonstrate that *Bcl2* is directly bound by Mll2 and indicates that the decreased expression is due to the absence of Mll2 regulation. Notably, the Mll2 binding region is in the second exon nearby the initiating methionine codon and coincident with a highly conserved noncoding element. Based on the *Bcl2* Vega annotation, the promoter seems to be at least 1-kb further 5′ upstream. The promoter region did not show Mll2 binding or decreased H3K4me^3 (data not shown). Hence, we suggest that Mll2 contributes to, but is not essential for, *Bcl2* expression.

Impaired Embryoid Body Formation in mll2−/− Cells

Embryoid bodies formed from *mll2*−/− cells were smaller than wild-type or FLP-rescued cells, and they were mis-

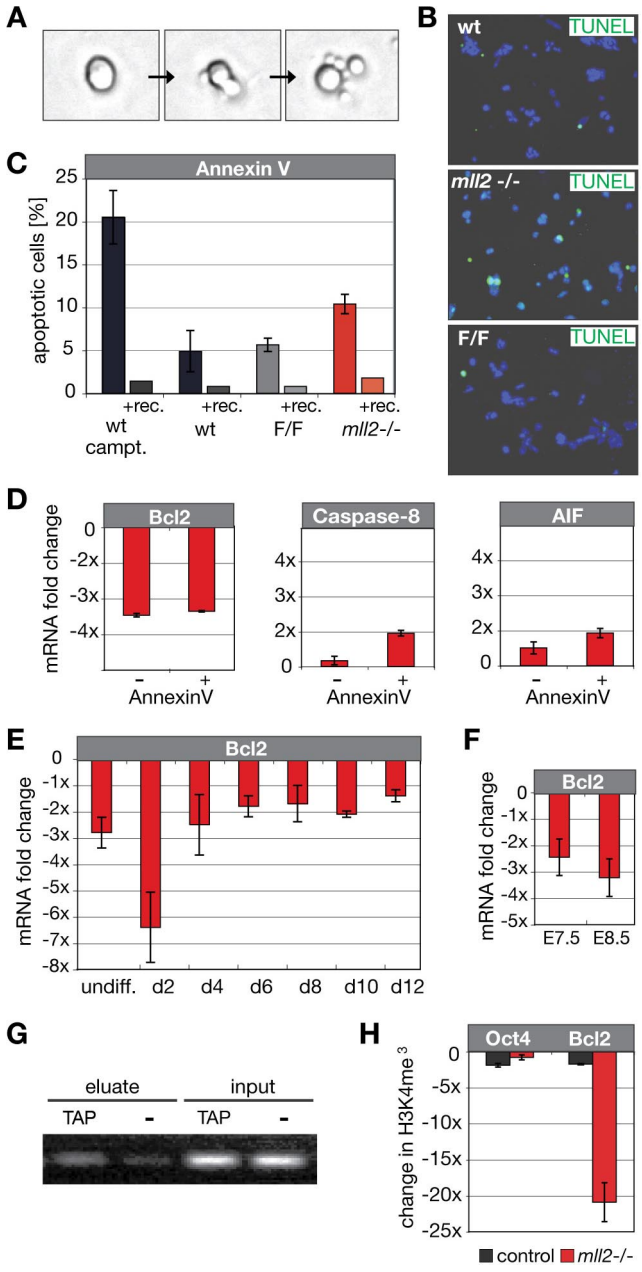

Figure 4. Enhanced rates of apoptosis in *mll2* mutant ES cells. (A) Tracking of mitotic cell divisions in time-lapse movies of asynchronous ES cell cultures. Detail screens from a time-lapse movie of *mll2*−/− ES cells indicate the occurrence of apoptotic cell death upon cell division. (B) Immunohistochemical detection of apoptosis in ES cell colonies based on enzymatic labeling of DNA strand breaks (TUNEL). Nuclei were counterstained with DAPI. (C) Apoptosis rates in wild-type, FLP-rescued, and *mll2*−/− ES cells determined by Annexin V flow cytometry. Left bars represent values for ES cell clones incubated with Annexin V-APC and PI; right bars indicate values for ES cells blocked with recombinant Annexin V protein (indicated as +rec.). Experiments were performed three times with similar results; data are means ± SD. Significance was determined by analysis of variance with a student's *t* test, $p < 0.025$. (D) Expression levels of apoptotic marker genes in *mll2* mutant cells. Apoptotic ES cells were separated from viable cell fractions by FACS sorting by using fluorescently labeled Annexin V-APC. Total RNA from both populations was isolated and quantitative PCR (qPCR) was performed to examine expression levels of pro- and antiapoptotic markers (*Bcl2*, anti-apoptotic; *Caspase-8* and *AIF*, pro-apoptotic). Graphs illustrate expression changes of respective genes in FACS-sorted viable [Annexin V (−)] and apoptotic [Annexin V (+)] *mll2*−/− ES cell populations compared with the average expression profile observed with wild-type and FLP-rescued ES cell fractions. (E) *Bcl2* expression profile in *mll2* mutant cells upon in vitro differentiation. ES cells were differentiated via mass culture of embryoid bodies and analyzed by qPCR at days indicated. Bars represent fold decrease of *Bcl2* expression in *mll2*−/− cells compared with wild-type and FLP-rescued cells. Analysis was performed in triplicates. (F) Decrease in *Bcl2* expression levels in early *mll2* mutant embryos compared with wild-type and heterozygous *mll2* +/− embryos. Embryos were dissected at embryonic day 7.5 or 8.5. For each time point, total RNA of three *mll2* +/+, +/−, and −/− embryos was reverse transcribed and used for qPCR analysis. Data are means of triplicate analysis ± SD. (G) Chromatin immunoprecipitation analysis for *Bcl2* on Mll2-TAP tagged ES cells. Cell lysates of Mll2-TAP ES cells were immunoprecipitated with IgG beads via the protein A of the TAP-tag. Untagged wild-type ES cells were used to determine background levels. DNA of input and immunoprecipitated eluates was PCR amplified with *Bcl2*-specific primers and separated by gel electrophoresis. (H) Chromatin immunoprecipitation of *mll2*−/− ES cells with H3K4me^3-specific antibodies. Heterozygous *mll2*+/− ES cells were used as a control. Expression levels of *Oct4* and *Bcl2* were determined by qPCR. Ct values were normalized against input DNA. Bars represent fold changes in H3K4me^3 between *mll2*−/− and wt ES cells. Error bar represent SD of triplicate analysis.

shapen (Figure 5A). Both wild-type and FLP-rescued embryoid bodies were round and smooth, whereas mutant embryoid bodies were irregular and rough. Doubling the number of seeded cells increased the aggregate size, but it did not alter the scrappy morphology.

Potentially, the defects in EB formation are caused solely by the increased rate of apoptosis. Because this increased rate is only moderate (at approximately 1 apoptosis per 20 cell divisions), we considered this unlikely. To gather more information on this issue, we looked at a variety of early markers in a simple differentiation time course via embryoid bodies (Figure 5B). All markers showed delayed kinetics throughout the time course, and doubling the number of starting cells did not rescue the delays. Because down-regulation of *Oct4* was also delayed, we conclude that *mll2*−/− cells are intrinsically slow to initiate differentiation.

mll2−/− Cells Are Delayed in Mesodermal and Ectodermal Differentiation

In vitro differentiation of ES cells yields cell types from all three primary germ layers. Here, we used in vitro differentiation into cardiac myocytes (mesoderm), neurons (ectoderm), and definitive endoderm to evaluate how Mll2 influences lineage commitment. Cardiac myocytes in embryoid body outgrowths were identified by labeling with cardiac-specific antibodies (Figure 5C) as well as by the presence of contractile activity (Figure 5D) and *brachyury* gene expression analysis (Figure 5B). Notably *mll2*−/− ES cells were able to differentiate almost as efficiently into cardiac myocytes as wild-type or FLP-rescued cells; however, the appearance of contractility occurred with a 3-d delay (Figure 5D). Because the differentiation capacity with this protocol is dependent on the number of cells differentiating in the embryoid bodies, we checked whether doubling the density of *mll2*−/− ES cells for embryoid body formation could restore the ability to differentiate into muscle. Although this slightly improved the efficiency of cardiac differentiation, it did not alter the delay. As expected, in wild-type cells expression of *brachyury*, an early mesodermal marker, peaked at day 3 and then diminished (Figure 5B). Notably, regula-

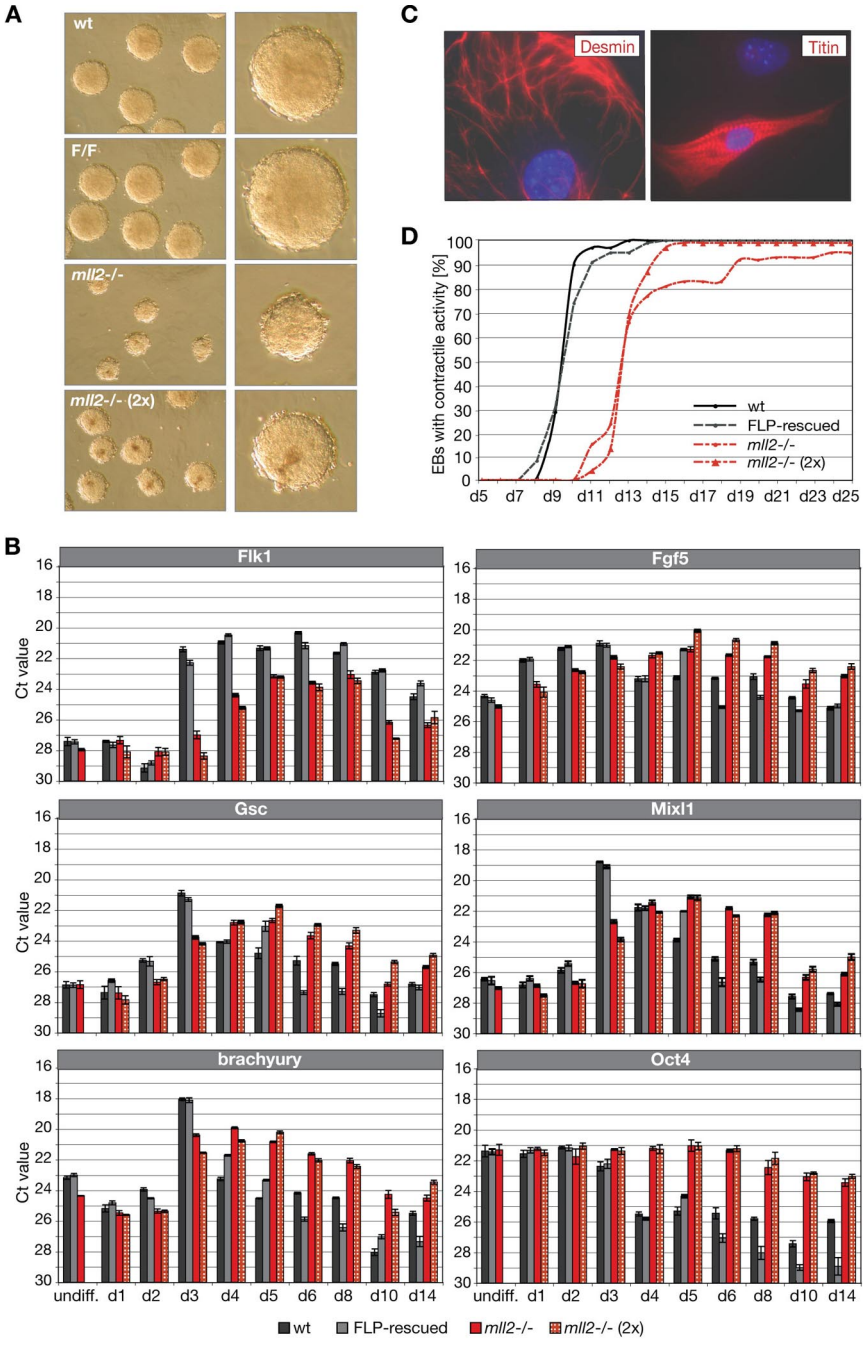

Figure 5. Cardiac differentiation of ES cells in vitro. (A) Embryoid body (EB) formation of wild-type, F/F, and *mll2*−/− ES cells on day 3 of cardiac in vitro differentiation, magnification 20× and close-up. EBs designated as *mll2*−/− (2x) were generated from 2 times more cells than the other three panels. (B) Quantitative expression analysis of early differentiation markers *Flk1* (early mesendoderm), *Gsc* and *Mixl1* (gastrulation), *Fgf5* (epiblast), *brachyury* (mesoderm), and the pluripotency marker *Oct4* upon cardiac in vitro differentiation. Total RNA from EBs at different time points was isolated and processed for reverse transcription. Ct values of qPCR analysis were normalized against *ribosomal protein L19* (*RPL19*). Data are means of triplicate analysis ± SD. (C) Regions of cardiogenesis were identified by appearance of cardiac specific markers. Contracting regions of *mll2* mutant ES cells were dissected, dissociated, and processed for cardiac-specific immunoreactivity by using anti-desmin and anti-titin antibodies. Magnification, 40×. (D) Appearance of spontaneous contractile activity during EB outgrowth. EBs, derived from a defined number of cells (1×10^3 cells/EB), were plated and checked for appearance of contractile activity (until day 25). In addition, *mll2*−/− EBs resulting from 2 times more cells (2×10^3 cells/EB) were monitored. Data were obtained from the same experimental series, n = 96 EBs.

tion of *brachyury* expression in *mll2*−/− cells was delayed, particularly for down-regulation. Whereas wild-type and FLP-rescued cells showed a drastic decrease on day 4 of differentiation, it took *mll2*−/− cells ~3 days longer to reduce their *brachyury* expression level.

In vitro differentiation toward neurons was identified by nestin immunofluorescence and later in postmitotic neurons by the presence of neuron-specific class III β-tubulin, MAP2 or 165-kDa neurofilament protein (NF-M). Although mature neurons were generated from Mll2-deficient cells, again a delay in differentiation became apparent (Figure 6A). All neurogenic markers tested by quantitative PCR were transcribed significantly less in Mll2-deficient cells throughout neuronal differentiation (Figure 6B). For *nestin*, the differences were relatively small, but markers for mature neurons showed striking differences in bulk expression levels. The average mRNA levels for class III β-tubulin or MAP2 on day 32 were ~14- or ~28-fold lower in mutants than in wild-type and FLP-rescued cells. Likewise, transcripts encoding the neuronal marker neurofilament protein 165-kDa (NF-M) showed drastic differences in abundance. NF-M is a marker for late neuronal development and confirmed the delay of *mll2* mutant cells upon differentiation. Transcripts for NF-M in *mll2* knockout cells on day 20 were ~35-fold and on day 24 more than ~50-fold less abundant than in wild-type and FLP-rescued cells at the same times. However, Mll2-deficient cells seem to catch up so that NF-M transcripts on day 32 were only approximately eightfold less abundant. In part

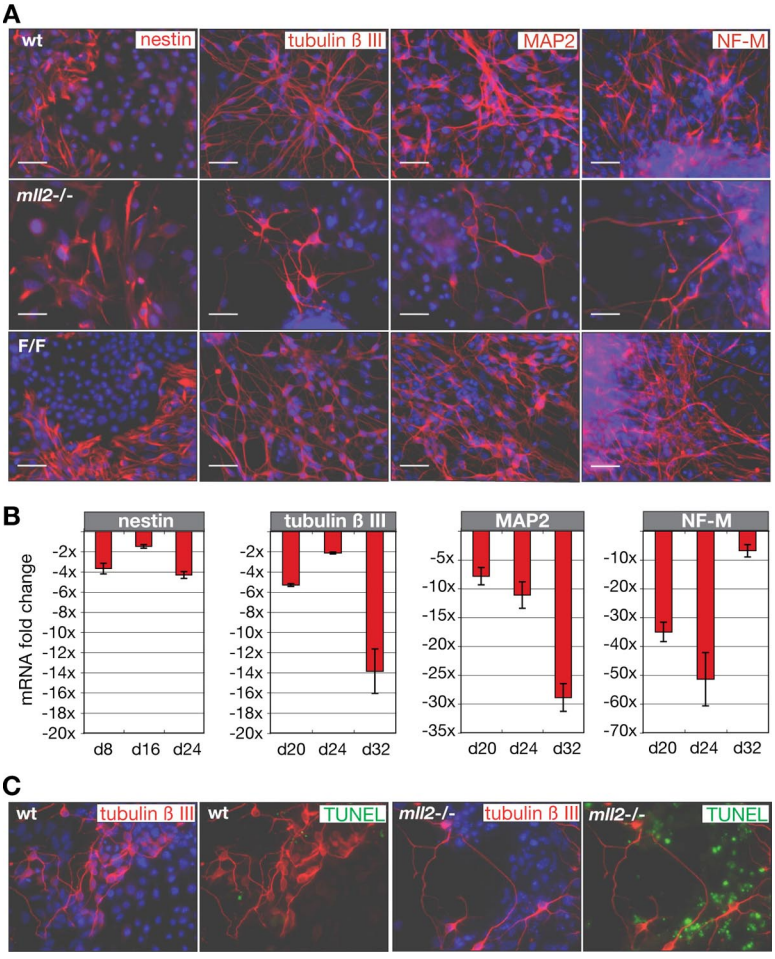

Figure 6. Neurogenic differentiation of ES cells in vitro. (A) Immunofluorescence analysis of wild-type, F/F, and *mll2*−/− cells for neuronal-specific markers (nestin, class III β-tubulin, MAP2, and 165-kDa neurofilament NF-M) at day 24 of neurogenic in vitro differentiation. Bar, 100 μm. (B) Quantification of neuronal marker gene expression at different time points upon neurogenic in vitro differentiation. Differential expression of early (nestin) and late neurogenic markers (class III β-tubulin, MAP2, neural cell adhesion molecule [NCAM], neurofilament NF-M) in *mll2*−/− cells compared with wild-type and FLP-rescued cells is shown. Except for *nestin* (day 8, day 16, and day 24) gene expression changes were determined on day 20, day 24, and day 32, respectively. Analyses were performed in triplicates and Ct values were normalized against the endogenous standard gene *ribosomal protein L19* (*RPL19*). Standard deviations of fold changes in normalized target gene expression are represented by error bars. (C) TUNEL staining of wild-type and *mll2*−/− cells on day 18 of neuronal in vitro differentiation. Combinatorial studies of TUNEL labeling with immunofluorescence analysis for neuron-specific class III β-tubulin, magnification 40×.

such disturbance of in vitro differentiation could be due to enhanced apoptosis levels in *mll2*−/− ES cells. TUNEL staining confirmed that *mll2*−/− cells continue to show an increased rate of apoptosis during differentiation (Figure 6C).

mll2−/− Cells Display Altered Endodermal Differentiation

Consistent with the delay in lineage commitment, *mll2*−/− cells also displayed a delay in down-regulation of the pluripotency marker gene *Oct4*. Normally, the Oct-4 POU transcription factor is rapidly down-regulated upon differentiation of ES cells (Niwa *et al*., 2000), and overexpression of *Oct4* drives endodermal differentiation (Palmieri *et al*., 1994). Higher expression levels of *Oct4* in *mll2*−/− cells could correlate with a bias toward endodermal differentiation. Quantitative PCR analysis revealed that *Oct4* transcripts in *mll2*−/− cells on day 12 of endodermal in vitro differentiation were approximately fivefold more abundant than in differentiating wild-type and FLP-rescued cells (Figure 7A). On day 15, this difference increased to ~12-fold. Nevertheless, in vitro differentiation of *mll2*−/− cells also showed an initial delay in differentiation toward endoderm. During the first 9 d of differentiation, the number of transcripts for two early endodermal markers, cytokeratin 8 (CK8) and hepatocyte nuclear factor 3 β (HNF3β), was slightly less in mutant cells. Later, *CK8* and *HNF3β* were expressed at same levels in wild-type and *mll2*−/− cells (Figure 7B), and markers for mature endodermal cell types, such as albumin 1 (ALB1) and α-fetoprotein (Afp), showed strongly increased expression (Figure 7B). In concordance with delayed *Oct4* down-regulation, expression levels of another pluripotency marker, *Nanog*, were elevated upon endodermal differentiation of *mll2*−/− cells as well (Figure 7A).

In summary, this study indicates that loss of Mll2 skews the timing of lineage commitment. Despite the fact that *mll2* mutant cells are slow to initiate differentiation, they proceed more successfully toward endodermal lineages.

DISCUSSION

Previously, we reported that *mll2*−/− embryos show growth retardation from E6.5 and subsequent developmental retardation leading to death by E11.5 (Glaser *et al*., 2006). Although evidence for specific defects in gene expression was observed, the simplest explanation for the embryonic lethal phenotype was elevated levels of apoptosis. Here, we report that *mll2*−/− ES cells also show enhanced apoptosis rates. Furthermore, we have been able to exploit the favorable properties of ES cells to examine the molecular basis of defects prompted by the loss of Mll2.

In comparison with parental or rescued ES cells, the *mll2*−/− ES cells did not show any differences in cell cycle distribution or cell cycle length. A moderate increase in the level of apoptosis affecting about 1 in 20 cell divisions was observed, which is sufficient to explain the observed slower rate of proliferation. This concords well with elevated apop-

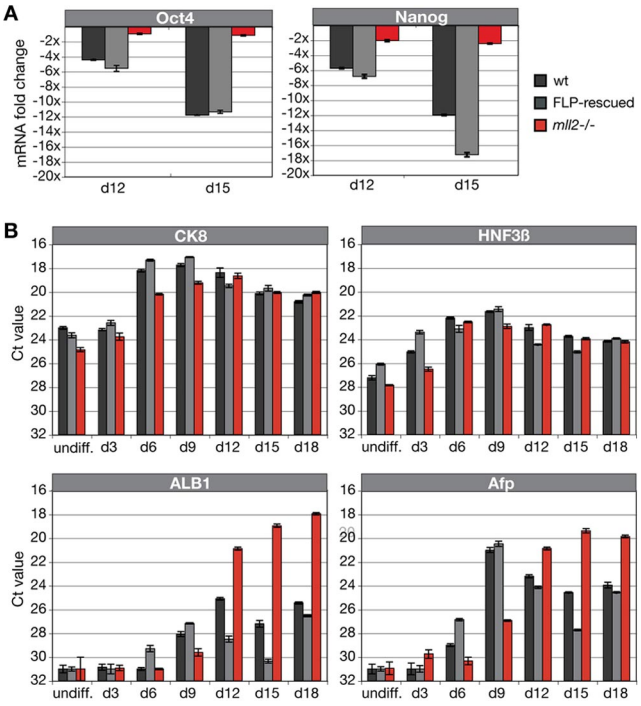

Figure 7. Endodermal differentiation of ES cell clones in vitro. (A) Quantitative PCR analysis of *Oct4* and *Nanog* gene expression upon in vitro differentiation into endoderm. Graphs illustrate expression changes of respective genes on day 12 or 15 relative to the undifferentiated state. Fold changes were calculated from *RPL19*-normalized Ct values; error bars represent SD of triplicate analysis. (B) Quantitative analysis of endoderm-specific transcripts in wild-type, F/F, and *mll2*−/− ES cells at different time points during endodermal in vitro differentiation. Expression levels of early endodermal markers, *cytokeratin 8* (*CK8*) and *hepatocyte nuclear factor 3 β* (*HNF3β*), and late endodermal markers, *albumin 1* (*ALB1*) and *α-fetoprotein* (*Afp*), were normalized against the internal standard gene *RPL19*. Data are means of triplicate analysis ± SD.

tosis and growth retardation during development as well as the cell autonomous character of the phenotype (Glaser *et al.*, 2006). We conclude that loss of Mll2 leads to increased apoptosis in many, if not all, cell types during development.

ES cells have two pathways linking mitochondria to apoptosis: one pathway that requires caspase activity (cytochrome *c*/Apaf1/caspase-9 apoptosome) (Li *et al.*, 1997), and another pathway that relies on the AIF operating in a caspase-independent manner (Daugas *et al.*, 2000). In viable cells, AIF protein is stored in the mitochondrial intermembrane space, from where it is released and transported into the nucleus in response to death stimuli (Susin *et al.*, 1999). It has been proposed that AIF accounts for initial apoptotic changes in the nucleus, whereafter cytochrome *c* triggers caspase activation, leading to advanced nuclear apoptosis (Daugas *et al.*, 2000). The AIF-dependent pathway is essential for controlled programmed cell death during early morphogenesis in mammals (Joza *et al.*, 2001). AIF action occurs caspase independently and is not inhibited by the general caspase inhibitor Z-VAD-FMK (Susin *et al.*, 1999). Moreover, AIF is released upon reduced levels of Bcl-2 protein, which typically preserves the integrity of mitochondrial membranes and protects cells from apoptosis (Marzo *et al.*, 1998; Daugas *et al.*, 2000) regardless of Apaf1 (Haraguchi *et al.*, 2000) or caspase activation (Amarante-Mendes *et al.*, 1998). Because we observed decreased *Bcl2* expression, a slight increase of AIF expression, and no rescue by Z-VAD-FMK inhibition of caspases in *mll2*−/− cells, we suggest that the increased apoptotic cell death is due to reduced Bcl2 protein levels and increased AIF release.

Notably Mll2 binds to the *Bcl2* gene and sustains H3K4me^3 around the 5′ end of the second exon, which is ~1 kb downstream of the annotated transcription start site. These observations are concordant with the observed moderate reduction of *Bcl2* expression, because we did not observe Mll2 binding or reduced H3K4me^3 at the annotated promoter. Whether this means that Mll2 is bound to an intragenic enhancer or to an alternative start site of *Bcl2* transcription remains to be determined. Besides, we conclude that Mll2 contributes to, but is not essential for, *Bcl2* expression.

Morphologically, *mll2*−/− ES cell colonies and embryoid bodies seem slightly disorganized, possibly due to the disruptive effects of sporadic cell elimination by apoptosis or lack of the cell surface SSEA1 antigen. Mutant ES cells show an almost complete loss of the stem cell marker SSEA1, which may be important for cell adhesion and proliferation (Cui *et al.*, 2004; Muramatsu and Muramatsu, 2004). SSEA1 is a carbohydrate antigen that is first expressed at the late eight-cell stage in mouse embryogenesis and becomes increased at later stages (Muramatsu and Muramatsu, 2004). This carbohydrate structure is postulated to be involved in tight adhesion of the blastomeres, a process called compaction (Fenderson *et al.*, 1984). Moreover, it has been proposed that carbohydrates participate in cell survival by enhancing the interaction of membrane molecules. Therefore, adhesion defects in Mll2-deficient cells, due to the loss of SSEA1, could add to the proliferative defect and contribute to discoordination of cell–cell communication. However, loss of SSEA1 expression did not impair pluripotency of *mll2* mutant ES cells.

Despite their proliferative defect, *mll2*−/− cells retain normal characteristics, form embryoid bodies, and differentiate toward all three germ lineages. This concords with the loss of function phenotype during development, which included progress past gastrulation and early organogenesis albeit with growth and developmental delays. It also concords with the maintenance model for transcriptional regulation, as exemplified by trxG and PcG action.

The maintenance model arose from studies on homeotic mutations in flies and differs from conventional regulation of gene expression, which relies on transcription factors binding to *cis*-acting sequence elements in promoters and enhancers. In trxG and PcG mutants, the expression of homeotic genes is established but not maintained (Ingham, 1983; Struhl and Akam, 1985; Heemskerk *et al.*, 1991), indicating that certain developmentally important genes are regulated by a two-stage mechanism. First, by the transcription factors that establish expression and second, by the recruitment of a mechanism involving trxG and PcG, which sustains gene expression. By recruiting this mechanism, the initial and inherently reversible mode of regulation by transcription factors is replaced by an epigenetic mode that secures inheritable maintenance of gene expression. Although it has gained a certain acceptance (Yu *et al.*, 1998), and credence from the connections between trxG, PcG, and histone 3 lysine methylation, the maintenance model has never been formalized in the literature and has been challenged recently (Brock and Fisher, 2005). Our data do not prove or disprove the model. However, they are concordant with it. Mll2 is not required for any of the complex changes in gene expression involved in the transition from pluripotency to differentiated states in all three germ layers, either in vitro as shown here or during development (Glaser *et al.*,

2006). Embryonic lethality occurs well after gastrulation and after the apparent failure to maintain the expression of certain homeobox genes, such as *Mox1* (Glaser *et al*., 2006). To the extent of published studies, the same can be said for its homologue Mll except with different target genes (Yagi *et al*., 1998; Yu *et al*., 1998; Hanson *et al*., 1999; Ernst *et al*., 2004).

Although Mll2 is not required for lineage commitment, the utility of ES cells allowed us to observe changes in timing. Differentiation toward all three germ layers was initially delayed. In the case of differentiation toward cardiac myocytes, a distinct 3-day delay was observed even when the protocol was initiated with twice the number of cells to compensate for loss due to apoptosis. In spite of the initial delay, differentiation to cardiac myocytes was quantitatively equivalent to wild type. Differentiation to neurons was not only delayed but also inefficient. In contrast, endodermal differentiation recovered from an initial delay to overshoot. Hence, we observe a complex imbalance in the temporal coordination of lineage commitment in the absence of Mll2. Whether this imbalance is solely due to increased apoptosis or indicates a role for Mll2 in the temporal coordination of lineage commitment remains to be established. Apparently, an increase in apoptosis upon withdrawal of LIF and the induction of differentiation has been observed (Duval *et al*., 2004). The same authors also showed that overexpression of *Bcl2* suppressed this apoptosis. However, it is not known whether Bcl2-mediated suppression of apoptosis is required for efficient differentiation.

Finally, we note that the observed complex imbalance in temporal coordination of differentiation offers an additional explanation for the *mll2*$-/-$ embryonic lethal phenotype. If similar imbalances were manifest during embryonic development, then the developmental failures could be due to the lack of reinforcing signals for pattern formation from cell–cell signaling. In addition to increased apoptosis or the maintenance model (Glaser *et al*., 2006), this presents a third possible explanation for the Mll2 embryonic phenotype, none of which are mutually exclusive.

ACKNOWLEDGMENTS

We thank Ina Nüsslein for assistance with FACS analysis, Frank Buchholz for help with time-lapse videomicroscopy, Imke Listermann for support with chromatin immunoprecipitation experiments, Pim Pijnappel for providing the E14.1 Mll2-TAP ES cells, Stefanie Weidlich for technical support, and Michelle Meredyth for discussions. This work was supported by funding from the 6th Research Framework Programme of the European Union, Project FunGenES (LSHG-CT-2003-503494), Project Heroic (LSHG-CT-2005-018883), and funding from the European Union, Freistaat Sachsen, and Technische Universität Dresden within the EFRE Project 4212/05-04. Desmin, titin, nestin, neurofilament NF-165, BrdU, and SSEA1 antibodies were obtained from the Developmental Studies Hybridoma Bank developed under the auspices of the National Institute of Child Health and Human Development and maintained by the Department of Biological Sciences (The University of Iowa, Iowa City, IA).

REFERENCES

Amarante-Mendes, G. P., Finucane, D. M., Martin, S. J., Cotter, T. G., Salvesen, G. S., and Green, D. R. (1998). Anti-apoptotic oncogenes prevent caspase-dependent and independent commitment for cell death. Cell Death Differ. *5*, 298–306.

Azuara, V., Perry, P., Sauer, S., Spivakov, M., Jorgensen, H. F., John, R. M., Gouti, M., Casanova, M., Warnes, G., Merkenschlager, M., and Fisher, A. G. (2006). Chromatin signatures of pluripotent cell lines. Nat. Cell Biol. *8*, 532–538.

Bernstein, B. E. *et al*. (2006). A bivalent chromatin structure marks key developmental genes in embryonic stem cells. Cell *125*, 315–326.

Boyer, L. A., Mathur, D., and Jaenisch, R. (2006a). Molecular control of pluripotency. Curr. Opin, Genet. Dev. *16*, 455–462.

Boyer, L. A. *et al*. (2006b). Polycomb complexes repress developmental regulators in murine embryonic stem cells. Nature *441*, 349–353.

Breen, T. R., and Harte, P. J. (1993). Trithorax regulates multiple homeotic genes in the bithorax and Antennapedia complexes and exerts different tissue-specific, parasegment-specific and promoter-specific effects on each. Development *117*, 119–134.

Brock, H. W., and Fisher, C. L. (2005). Maintenance of gene expression patterns. Dev. Dyn. *232*, 633–655.

Cao, R., Wang, L., Wang, H., Xia, L., Erdjument-Bromage, H., Tempst, P., Jones, R. S., and Zhang, Y. (2002). Role of histone H3 lysine 27 methylation in Polycomb-group silencing. Science *298*, 1039–1043.

Cui, L., Johkura, K., Yue, F., Ogiwara, N., Okouchi, Y., Asanuma, K., and Sasaki, K. (2004). Spatial distribution and initial changes of SSEA-1 and other cell adhesion-related molecules on mouse embryonic stem cells before and during differentiation. J. Histochem. Cytochem. *52*, 1447–1457.

Czermin, B., Melfi, R., McCabe, D., Seitz, V., Imhof, A., and Pirrotta, V. (2002). *Drosophila* enhancer of Zeste/ESC complexes have a histone H3 methyltransferase activity that marks chromosomal Polycomb sites. Cell *111*, 185–196.

Daugas, E., Susin, S. A., Zamzami, N., Ferri, K. F., Irinopoulou, T., Larochette, N., Prevost, M. C., Leber, B., Andrews, D., Penninger, J., and Kroemer, G. (2000). Mitochondrio-nuclear translocation of AIF in apoptosis and necrosis. FASEB J. *14*, 729–739.

Dodge, J. E., Kang, Y. K., Beppu, H., Lei, H., and Li, E. (2004). Histone H3–K9 methyltransferase ESET is essential for early development. Mol. Cell. Biol. *24*, 2478–2486.

Duval, D., Malaise, M., Reinhardt, B., Kedinger, C., and Boeuf, H. (2004). A p38 inhibitor allows to dissociate differentiation and apoptotic processes triggered upon LIF withdrawal in mouse embryonic stem cells. Cell Death Differ. *11*, 331–341.

Ernst, P., Fisher, J. K., Avery, W., Wade, S., Foy, D., and Korsmeyer, S. J. (2004). Definitive hematopoiesis requires the mixed-lineage leukemia gene. Dev. Cell *6*, 437–443.

Fenderson, B. A., Zehavi, U., and Hakomori, S. (1984). A multivalent lacto-N-fucopentaose III-lysyllysine conjugate decompacts preimplantation mouse embryos, while the free oligosaccharide is ineffective. J. Exp. Med. *160*, 1591–1596.

Glaser, S., Schaft, J., Lubitz, S., Vintersten, K., van der Hoeven, F., Tufteland, K. R., Aasland, R., Anastassiadis, K., Ang, S. L., and Stewart, A. F. (2006). Multiple epigenetic maintenance factors implicated by the loss of Mll2 in mouse development. Development *133*, 1423–1432.

Hakem, R. *et al*. (1998). Differential requirement for caspase 9 in apoptotic pathways in vivo. Cell *94*, 339–352.

Hanson, R. D. *et al*. (1999). Mammalian Trithorax and polycomb-group homologues are antagonistic regulators of homeotic development. Proc. Natl. Acad. Sci. USA *96*, 14372–14377.

Haraguchi, M., Torii, S., Matsuzawa, S., Xie, Z., Kitada, S., Krajewski, S., Yoshida, H., Mak, T. W., and Reed, J. C. (2000). Apoptotic protease activating factor 1 (Apaf-1)-independent cell death suppression by Bcl-2. J. Exp. Med. *191*, 1709–1720.

Heemskerk, J., DiNardo, S., Kostriken, R., and O'Farrell, P. H. (1991). Multiple modes of engrailed regulation in the progression towards cell fate determination. Nature *352*, 404–410.

Ingham, P. W. (1983). Differential expression of bithorax complex genes in the absence of the extra sex combs and trithorax genes. Nature *306*, 591–593.

Joza, N. *et al*. (2001). Essential role of the mitochondrial apoptosis-inducing factor in programmed cell death. Nature *410*, 549–554.

Kluck, R. M., Bossy-Wetzel, E., Green, D. R., and Newmeyer, D. D. (1997). The release of cytochrome c from mitochondria: a primary site for Bcl-2 regulation of apoptosis. Science *275*, 1132–1136.

Klymenko, T., and Muller, J. (2004). The histone methyltransferases Trithorax and Ash1 prevent transcriptional silencing by Polycomb group proteins. EMBO Rep. *5*, 373–377.

Kudo, T., Kaneko, M., Iwasaki, H., Togayachi, A., Nishihara, S., Abe, K., and Narimatsu, H. (2004). Normal embryonic and germ cell development in mice lacking alpha 1,3-fucosyltransferase IX (Fut9) which show disappearance of stage-specific embryonic antigen 1. Mol. Cell. Biol. *24*, 4221–4228.

Kuzmichev, A., Nishioka, K., Erdjument-Bromage, H., Tempst, P., and Reinberg, D. (2002). Histone methyltransferase activity associated with a human multiprotein complex containing the Enhancer of Zeste protein. Genes Dev. *16*, 2893–2905.

Lee, T. I. *et al*. (2006). Control of developmental regulators by Polycomb in human embryonic stem cells. Cell *125*, 301–313.

Li, M., Pevny, L., Lovell-Badge, R., and Smith, A. (1998). Generation of purified neural precursors from embryonic stem cells by lineage selection. Curr. Biol. *8*, 971–974.

Li, P., Nijhawan, D., Budihardjo, I., Srinivasula, S. M., Ahmad, M., Alnemri, E. S., and Wang, X. (1997). Cytochrome c and dATP-dependent formation of Apaf-1/caspase-9 complex initiates an apoptotic protease cascade. Cell *91*, 479–489.

Lin, W., and Dent, S. Y. (2006). Functions of histone-modifying enzymes in development. Curr. Opin. Genet. Dev. *16*, 137–142.

Liu, N., Jin, C., Zhu, Z. M., Zhang, J., Tao, H., Ge, C., Yang, S., and Zhang, S. (1999). Stage-specific expression of alpha1,2-fucosyltransferase and alpha1, 3-fucosyltransferase (FT) during mouse embryogenesis. Eur. J. Biochem. *265*, 258–263.

Livak, K. J., and Schmittgen, T. D. (2001). Analysis of relative gene expression data using real-time quantitative PCR and the 2(-Delta Delta C(T)) method. Methods *25*, 402–408.

Lumelsky, N., Blondel, O., Laeng, P., Velasco, I., Ravin, R., and McKay, R. (2001). Differentiation of embryonic stem cells to insulin-secreting structures similar to pancreatic islets. Science *292*, 1389–1394.

Maltsev, V. A., Rohwedel, J., Hescheler, J., and Wobus, A. M. (1993). Embryonic stem cells differentiate in vitro into cardiomyocytes representing sinus-nodal, atrial and ventricular cell types. Mech. Dev. *44*, 41–50.

Margueron, R., Trojer, P., and Reinberg, D. (2005). The key to development: interpreting the histone code? Curr. Opin. Genet. Dev. *15*, 163–176.

Marzo, I., Brenner, C., Zamzami, N., Susin, S. A., Beutner, G., Brdiczka, D., Remy, R., Xie, Z. H., Reed, J. C., and Kroemer, G. (1998). The permeability transition pore complex: a target for apoptosis regulation by caspases and bcl-2-related proteins. J. Exp. Med. *187*, 1261–1271.

Meshorer, E., and Misteli, T. (2006). Chromatin in pluripotent embryonic stem cells and differentiation. Nat. Rev. *7*, 540–546.

Milne, T. A., Briggs, S. D., Brock, H. W., Martin, M. E., Gibbs, D., Allis, C. D., and Hess, J. L. (2002). MLL targets SET domain methyltransferase activity to Hox gene promoters. Mol. Cell. *10*, 1107–1117.

Muller, J., Hart, C. M., Francis, N. J., Vargas, M. L., Sengupta, A., Wild, B., Miller, E. L., O'Connor, M. B., Kingston, R. E., and Simon, J. A. (2002). Histone methyltransferase activity of a *Drosophila* Polycomb group repressor complex. Cell *111*, 197–208.

Muramatsu, T. (1988). Developmentally regulated expression of cell surface carbohydrates during mouse embryogenesis. J. Cell Biochem. *36*, 1–14.

Muramatsu, T., and Muramatsu, H. (2004). Carbohydrate antigens expressed on stem cells and early embryonic cells. Glycoconj. J. *21*, 41–45.

Nichols, J., Zevnik, B., Anastassiadis, K., Niwa, H., Klewe-Nebenius, D., Chambers, I., Scholer, H., and Smith, A. (1998). Formation of pluripotent stem cells in the mammalian embryo depends on the POU transcription factor Oct4. Cell *95*, 379–391.

Niwa, H., Miyazaki, J., and Smith, A. G. (2000). Quantitative expression of Oct-3/4 defines differentiation, dedifferentiation or self-renewal of ES cells. Nat. Genet. *24*, 372–376.

Palmieri, S. L., Peter, W., Hess, H., and Scholer, H. R. (1994). Oct-4 transcription factor is differentially expressed in the mouse embryo during establishment of the first two extraembryonic cell lineages involved in implantation. Dev. Biol. *166*, 259–267.

Ringrose, L., and Paro, R. (2004). Epigenetic regulation of cellular memory by the Polycomb and Trithorax group proteins. Annu. Rev. Genet. *38*, 413–443.

Roguev, A., Schaft, D., Shevchenko, A., Pijnappel, W. W., Wilm, M., Aasland, R., and Stewart, A. F. (2001). The *Saccharomyces cerevisiae* Set1 complex includes an Ash2 homologue and methylates histone 3 lysine 4. EMBO J. *20*, 7137–7148.

Schaft, J., Ashery-Padan, R., van der Hoeven, F., Gruss, P., and Stewart, A. F. (2001). Efficient FLP recombination in mouse ES cells and oocytes. Genesis *31*, 6–10.

Solter, D., and Knowles, B. B. (1978). Monoclonal antibody defining a stage-specific mouse embryonic antigen (SSEA-1). Proc. Natl. Acad. Sci. USA *75*, 5565–5569.

Struhl, G., and Akam, M. (1985). Altered distributions of Ultrabithorax transcripts in extra sex combs mutant embryos of *Drosophila*. EMBO J. *4*, 3259–3264.

Susin, S. A. *et al*. (1999). Molecular characterization of mitochondrial apoptosis-inducing factor. Nature *397*, 441–446.

Tachibana, M. *et al*. (2002). G9a histone methyltransferase plays a dominant role in euchromatic histone H3 lysine 9 methylation and is essential for early embryogenesis. Genes Dev. *16*, 1779–1791.

Testa, G., Schaft, J., van der Hoeven, F., Glaser, S., Anastassiadis, K., Zhang, Y., Hermann, T., Stremmel, W., and Stewart, A. F. (2004). A reliable lacZ expression reporter cassette for multipurpose, knockout-first alleles. Genesis *38*, 151–158.

Testa, G., Zhang, Y., Vintersten, K., Benes, V., Pijnappel, W. W., Chambers, I., Smith, A. J., Smith, A. G., and Stewart, A. F. (2003). Engineering the mouse genome with bacterial artificial chromosomes to create multipurpose alleles. Nat. Biotechnol. *21*, 443–447.

Woo, M. *et al*. (1998). Essential contribution of caspase 3/CPP32 to apoptosis and its associated nuclear changes. Genes Dev. *12*, 806–819.

Yagi, H., Deguchi, K., Aono, A., Tani, Y., Kishimoto, T., and Komori, T. (1998). Growth disturbance in fetal liver hematopoiesis of Mll-mutant mice. Blood *92*, 108–117.

Ying, Q. L., Stavridis, M., Griffiths, D., Li, M., and Smith, A. (2003). Conversion of embryonic stem cells into neuroectodermal precursors in adherent monoculture. Nat. Biotechnol. *21*, 183–186.

Yoshida, H., Kong, Y. Y., Yoshida, R., Elia, A. J., Hakem, A., Hakem, R., Penninger, J. M., and Mak, T. W. (1998). Apaf1 is required for mitochondrial pathways of apoptosis and brain development. Cell *94*, 739–750.

Yu, B. D., Hanson, R. D., Hess, J. L., Horning, S. E., and Korsmeyer, S. J. (1998). MLL, a mammalian trithorax-group gene, functions as a transcriptional maintenance factor in morphogenesis. Proc. Natl. Acad. Sci. USA *95*, 10632–10636.

Yu, S. W., Wang, H., Poitras, M. F., Coombs, C., Bowers, W. J., Federoff, H. J., Poirier, G. G., Dawson, T. M., and Dawson, V. L. (2002). Mediation of poly(ADP-ribose) polymerase-1-dependent cell death by apoptosis-inducing factor. Science *297*, 259–263.

Zhang, Y., Buchholz, F., Muyrers, J. P., and Stewart, A. F. (1998). A new logic for DNA engineering using recombination in *Escherichia coli*. Nat. Genet. *20*, 123–128.